J. Fluid Mech. (1972), *vol.* 55, *part* 1, *pp.* 65–92
Printed in Great Britain

Structure of the Reynolds stress near the wall

By W. W. WILLMARTH AND S. S. LU
Department of Aerospace Engineering, The University of Michigan

(Received 13 December 1971)

Experimental studies of the flow field near the wall in a turbulent boundary layer using hot-wire probes are reported. Measurements of the product uv are studied using the technique of conditional sampling with a large digital computer to single out special events (bursting) when large contributions to turbulent energy and Reynolds stress occur. The criterion used to determine when the product uv is sampled is that the streamwise velocity at the edge of the sublayer should have attained a certain value. With this simple criterion we find that 60 % of the contribution to $\overline{uv}$ is produced when the sublayer velocity is lower than the mean. This result is true at both low, $R_\theta = 4230$, and high, $R_\theta = 38000$, Reynolds numbers. With a more strict sampling criterion, that the filtered sublayer velocity at two side-by-side points should be simultaneously low and decreasing, individual contributions to $\overline{uv}$ as large as 62 $\overline{uv}$ have been identified. Additional measurements using correlations between truncated u and v signals reveal that the largest contributions to the Reynolds stress and turbulent energy occur when $u < 0$, $v > 0$ during an intense bursting process and the remainder of the contributions occur during a less intense recovery process. Thus, contributions to the turbulent energy production and Reynolds stress at a point near the wall are of relatively large magnitude, short duration and occur intermittently. A rough measure of the intermittency factor for uv at a point near the wall is 0·55 since 99 % of the contribution to $\overline{uv}$ is made during only 55 % of the total time.

1. Introduction

This paper is a report of an experimental study of the nature of the unsteady flow near the wall that is responsible for the Reynolds stress which develops in the boundary layer on a smooth flat plate. Information about the flow field in the region near the wall is of great importance for a proper understanding of the structure of turbulence in the boundary layer. Just outside the sublayer in the region $20 < y^+ < 200$† the Reynolds stress and the turbulent kinetic energy are a maximum. Somewhat nearer the wall, at $y^+ \simeq 10$, the production and dissipation of turbulent kinetic energy are a maximum. Based upon local mean values the turbulent kinetic energy is a maximum of roughly 20 % of the local mean kinetic energy at approximately $y^+ = 15$ and maintains a high value, greater than 12 % of the local mean kinetic energy, all the way to the wall, within the sublayer.

In the past fifteen years, there have been numerous studies of the turbulent

† The superscript + indicates the dimensionless length $y^+ = y(\tau_w/\rho)^{\frac{1}{2}}/\nu$.

flow field near the wall. We do not have the space for a comprehensive review and will confine our discussion to recent papers and results pertinent to the present investigation of the structure of the Reynolds stress. The primary motivation for the present work on turbulent structure was provided by the studies of Kim, Kline & Reynolds (1968), the work of Corino & Brodkey (1969) and by our interest in a model for the turbulent structure near the wall, Willmarth & Tu (1967).

The recent studies by Kim *et al.* (1968) show that the low-speed fluid in the region near the wall occasionally erupts violently into the high-speed outer region of the boundary layer. Following Kim *et al.* this process is called bursting. During the bursting process Kim *et al.* estimated (from the trajectories of small hydrogen bubbles) the rate of production of turbulent energy. They concluded that "essentially all the turbulent production occurs during bursting periods in the zone $0 < y^+ < 90$". The bursting process, as described by Kim *et al.*, began with a lifting motion of a streak or filament of low-speed fluid within the sublayer. The streaks of low-speed fluid were identified by filamentary concentrations of tracer particles introduced into the fluid very near the wall. When the rising filament of low-speed fluid reached a height in the range $8 < y^+ < 12$, an oscillatory motion of marked fluid lines (time lines) within the parcel was observed. The oscillatory motions, which were of various types, appeared to be associated with a swirling motion of the fluid. As the amplitude of the swirling motion of the rising fluid became larger, the pattern 'broke up' at a distance from the wall in the range $10 < y^+ < 40$. During the breakup process, a significantly more random chaotic motion occurred in which marked lines of fluid were obliterated owing to the sudden increase in turbulent mixing.

The detailed observations of Kim *et al.* were obtained by marking the fluid (water) passing over a slender wire normal or parallel to the wall. A succession of current pulses passing from the water into the wire caused electrolysis of the water and subsequent deposition of lines of small hydrogen bubbles in the water moving past the wire. The motion of the lines of bubbles could be observed until the breakup process occurred. After breakup the bubble concentration was reduced and further observation was not possible. In this way, a significantly greater amount of qualitative information about the flow field near the wall was obtained than had ever been available before.

Corino & Brodkey (1969) used a high-speed motion-picture camera to photograph the trajectories of very small particles suspended in the flow. The camera was mounted on a traversing mechanism so that the motions within the convected flow structure responsible for the bursting phenomena could be kept in view as the pattern was swept downstream. The observations of the bursting phenomena reported by Corino & Brodkey are in essential agreement with those reported by Kim *et al.* However, Corino & Brodkey observed the motion of all the fluid particles passing through the field of view of the camera. They were able to identify additional features of the breakup process and the flow after breakup that could not be observed by marking only the fluid elements that passed over the upstream bubble-generating wire used by Kim *et al.*

The sequence of events before and after chaotic breakdown during the bursting

process reported by Corino & Brodkey began with the formation of a low-speed parcel of fluid near the wall, for $0 < y^+ < 30$. The velocity of the low-speed region was often as low as 50 % of the local mean velocity with a very small streamwise velocity gradient within the low-speed region. After a low-speed region had formed the next step occurred, and was called acceleration by Corino & Brodkey. During acceleration a much larger scale high-speed parcel of fluid came into view and by 'interaction' began to accelerate the fluid.

At various times the entering high-speed fluid appeared to occupy the same region on the photograph as the low-speed fluid. The explanation is that the high-speed region was within the field of view but at a different spanwise station to one side or the other of the low-speed parcel of fluid. It appears to us that the spanwise variation revealed by the above observation may be related to the observation of a streaky structure within the sublayer reported by Kline, Reynolds, Schraub & Runstadler (1967). This is supported by the fact that the depth of field was of the right order of magnitude, $z^+ \simeq 20$, to allow observation of a single transverse shear layer formed by adjacent high- and low-speed regions near the wall where the streaks have a typical spanwise spacing of $z^+ = 100$.

Continuing with the description of the acceleration phase, if the high- and low-speed fluid met at the same spanwise station, the interaction was often immediate; the low-speed fluid above a particular y^+ location was accelerated and a very sharp interface or shear layer between accelerated and retarded fluid was formed. The next step in the process was called ejection by Corino & Brodkey. During ejection one or more eruptions of low-speed fluid occurred immediately or shortly after the start of the acceleration process. Once ejection began, the process proceeded rapidly to a fully developed stage during which ejection of low-speed fluid persisted for varying periods of time and then gradually ceased. The length scale of ejected fluid elements was small, of the order of $7 < z^+ < 20$ and $20 < x^+ < 40$. Most of the ejections occurred at distances from the wall in the range $5 < y^+ < 15$. When the ejected low-speed fluid encountered the interface between high- and low-speed fluid, at the high shear layer, a violent interaction occurred with intense, abrupt and chaotic movements. The intense interaction continued as more fluid was ejected. The end result was the creation of a relatively large-scale region of turbulent motion reaching into the sublayer as the violent interaction region spread out in all directions.

The ejection or bursting phase ended with the entry from further upstream of fluid directed primarily in the stream direction with a velocity approximating the normal mean velocity profile. The entering high-speed fluid carried away the retarded fluid remaining from the ejection process and this was called the sweep event by Corino & Brodkey.

Both Corino & Brodkey and Kim *et al.* agree that the bursting phenomena is an important process for turbulent energy production. Corino & Brodkey conclude that "the results do indicate that the ejections are very energetic and well correlated so as to be a major contributor to the Reynolds stress and thus the production of turbulent energy". Their rough estimates of the Reynolds stress contribution during bursting from a small sample of bursting events indicated that 70 % of the Reynolds stress was produced during ejections.

Using the above information as a background we have designed a number of experiments using hot-wire anemometers to make quantitative measurements of the flow field near the wall. The experiments are designed to provide additional information about the turbulent velocity field that is difficult to obtain with flow visualization methods. It should be noted that fluid velocity measurements at a given point in the flow cannot be made using photographs of bubble trajectories downstream of the bubble-generating wire unless the bubbles happen to pass through the given point. Also, fluid velocity measurements at a given point in the flow cannot be made using the motion-picture photographs of numerous small suspended particles unless the depth of field can be made very small relative to the dimensions of the flow field in question. In Corino & Brodkey's photographs the depth of field was small, of order $z^+ = 20$, which is as large as the typical size of an ejected region of low-speed fluid near the wall.

The experiments that are discussed in the body of this report consist primarily of various fluid velocity measurements near the wall which we have made during the past few years. The measurements show substantial agreement with the process of bursting as observed and described by Kim *et al.* and by Corino & Brodkey. We are able to give quantitative support to the statement that the bursting process is important for the production of turbulent energy. In addition, the above flow visualization results for the bursting process and the results of our present measurements and of our previous pressure–velocity correlation measurements (Willmarth & Wooldridge 1963) all agree with a simplified model which we have proposed (Willmarth & Tu 1967) for the turbulent structure near the wall.

2. Experimental apparatus and methods

The experiments were conducted in a thick turbulent boundary layer developed on the smooth floor of the 5×7 ft low-speed wind tunnel of the Department of Aerospace Engineering at the University of Michigan. Some pertinent characteristics of this facility are discussed by Willmarth & Wooldridge (1962).

2.1. *Mean boundary-layer characteristics*

Most of the detailed measurements were done in a boundary layer with a thick sublayer that is produced at low free-stream speeds, $U_\infty \simeq 20$ ft/s. Some measurements were also made at higher free-stream speeds, $U_\infty \simeq 200$ ft/s; in this case the sublayer is much thinner. Owing to the small scale of the bursting phenomena near the wall, we preferred to use the boundary layer with as large a sublayer thickness as possible but found that at very low speeds $5 < U_\infty < 10$ ft/s, with natural transition, the turbulent boundary layer was not fully developed at the rearmost station, $x = 35$ ft, of the test section. The lowest possible speed was 20 ft/s.

Typical mean velocity profiles measured with an impact pressure tube and with a hot wire are displayed in figure 1, and table 1 lists the pertinent parameters for the two fully developed flat-plate boundary layers. The wall shear stress was measured using the Clauser plot (Clauser 1956), see figure 1. We emphasize here

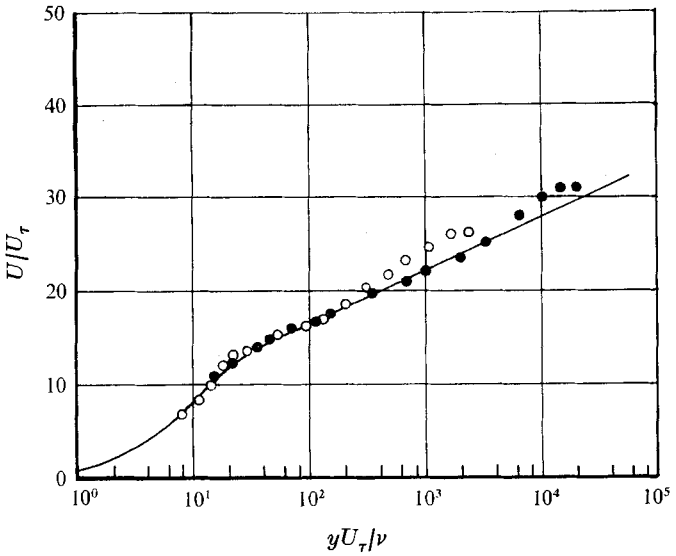

FIGURE 1. Mean velocity profiles: ○, U_∞ = 19·7 ft/s; ●, U_∞ = 204 ft/s. (See also table 1.)

U_∞ (ft/s)	R_θ	δ (ft)	δ^* (ft)	θ (ft)	δ^*/θ	U_τ/U_∞	R_x	Remarks
19·7	4230	0·405	0·0494	0·0363	1·365	0·0386		Transition: location not known
—	3800	—	—	—	1·383	0·0387	$2·1 \times 10^6$	Cole's ideal boundary layer
204	38000	0·42	0·041	0·0315	1·30	0·0326	$3·1 \times 10^7$	See Willmarth & Tu (1966)
—	39000	—	—	—	1·30	0·0318	$3·2 \times 10^7$	Cole's ideal boundary layer

TABLE 1. Properties of the actual and ideal turbulent boundary layer (as tabulated by Coles (1954))

that artificial tripping and roughness were not used because we did not want to introduce additional unnatural flow disturbances which might not die out before reaching the measurement station. We believe that flow structure measurements and/or measurements of fluctuating quantities are more sensitive to artificial upstream disturbances than are measurements of mean quantities.

2.2. *Hot-wire anemometer probes*

Measurements were made with hot-wire anemometer probes of various types. The measurements of streamwise velocity very near the wall were made with platinum wires of diameter $1·5 \times 10^{-4}$ in. The wires were glued directly on the wall 0·002 in. from the surface and were 0·032 in. long for the high-speed measurements. For low-speed measurements the wires were soldered to the tips of needles protruding through the wall. The wires used at low speeds were 0·037 in. from the wall with lengths of 0·10 in. and 0·045 in. These wires were made by etching the silver away from platinum wire, soldering the wire to one needle tip and

letting it hang, with a small weight on the end, near the lower needle tip. Then the hanging wire was soldered to the lower needle tip. The surface tension of the molten solder was very effective in pulling the wire onto the needle tip.

The streamwise vorticity component was measured using a scheme described by Kovasznay (1954). The probe was constructed by Dr Bo Jang Tu in 1968 using four 2×10^{-4} in. diameter tungsten wires which were copper plated before being soldered to the four-needle probe. Careful matching of the resistance of the four wires using a process of etching of copper from individual wires made the probe insensitive to velocity fluctuations of a scale larger than the probe. The etching process was accomplished using a tiny bubble of copper sulphate solution suspended in a loop of thin platinum wire. The wires were matched so that the difference in the resistance of the four wires was less than 3 % of the nominal wire resistance. The probe was calibrated using a specially constructed oscillating mechanism and gave a linear response to the imposed vorticity caused by rotating the probe about its streamwise axis.

The Reynolds stress was measured using the usual X-wire configuration of 2×10^{-4} in. diameter copper-plated tungsten wires. Each wire was soldered on needles 0·07 in. apart at angles of $\pm 45°$ to the flow. The distance between the wire centres was 0·04 in. and the wires were 0·035 in. long. The wire resistance was approximately 3 ohms when cold and the difference in resistance between a pair of wires was less than 3 % of the nominal wire resistance.

2.3. *Hot-wire anemometer equipment*

The hot-wire signals were processed using both constant-current and constant-temperature equipment. The electrical signals from the vorticity probes and the X-wire probes were obtained when the wires were heated using the constant-current method. The signals were amplified and compensated using techniques described by Kovasznay (1954).

In the case of the streamwise vorticity probe the four wires were connected in a Wheatstone bridge configuration with a constant current supply across two arms of the bridge and the input of an amplifier across the other two arms. In our system we used a Shapiro & Edwards amplifier and compensator which has one side of the input grounded. The constant current supply was obtained from a pack of batteries isolated from the ground.

Each wire of the X-wire probe was separately heated at constant current and a separate channel of amplification and compensation was used for each wire. The wires, amplifier gain, and amount of compensation in each channel were carefully matched so that they were identical, within a few per cent. Each wire was separately calibrated in a steady laminar flow at various velocities. The calibrations differed by less than 3 % and obeyed King's law with good accuracy. The wires were operated at an overheating ratio of one half. The time constant of each wire was approximately $9{\cdot}5 \times 10^{-4}$ s near the wall in the low-speed boundary layer and 5×10^{-4} s in the high-speed boundary layer. The above values represent the maximum amount of compensation necessary near the wall. We carefully compared the gain and phase shift of each channel with compensation networks operating over the entire frequency band, $1 < f < 20\,000$ Hz, using

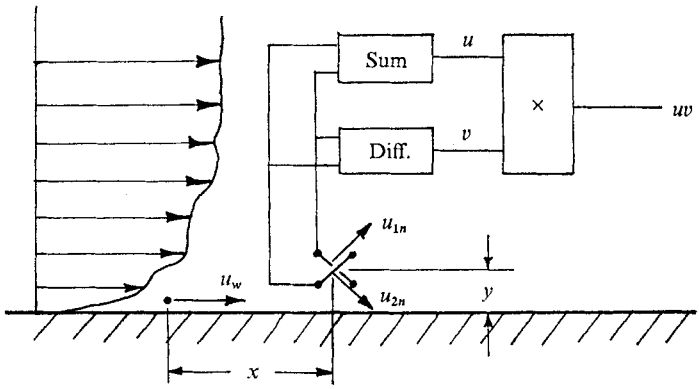

FIGURE 2. Sketch of arrangement of hot wires for measurement of u_w and uv.

a Lissajous figure displayed on matched x and y channels of a Hewlett Packard oscilloscope. The gain and phase shift did not differ by more than 3 % over the entire bandwidth.

The streamwise velocity signal at the edge of the sublayer used for conditional sampling measurements was produced with a Miller constant-temperature hot-wire set or occasionally with a Disa Model 55 D05 constant-temperature hot-wire set. The Miller hot-wire set is based on a design reported by Kovasznay *et al.* (1963). We did not use linearizers for the hot-wire signal u_w from wires in the sublayer. We know that some error in the signal u_w is thus introduced. However, the signal u_w representing streamwise sublayer velocity was only used to determine the condition of the sublayer in the conditional sampling measurements.

2.4. *Other electronic equipment*

The signals obtained from the hot wires were recorded on magnetic tape using a frequency modulated system installed in a three-channel Ampex Model FR-1100 tape recorder. We also used a six-channel Ampex Model 300 A recorder with the same frequency modulated electronic system. The analog data were stored on reels of magnetic tape and could be played back later at faster or slower speeds.

The initial data reduction was accomplished using an analog scheme. We constructed a small analog computer to compute the Reynolds stress from the signals produced by the two wires on the X-probe. The scheme is outlined in figure 2. The summing amplifier was a Fairchild ADO-25 and the multiplier was an Intronics Model M502 wide-band analog multiplier. The analog computation was accurate within 1 % in amplitude and phase in the range $0 < f < 20000$ Hz.

The Reynolds stress signal from the multiplier was detected by a Princeton Applied Research Model TDH-9 Wave Form Eductor. The sampling cycle of the wave form eductor was triggered by a signal derived from a comparitor and pulse-shaping circuit made up from Fairchild 2N2422 and 2N3904 transistors. We gratefully acknowledge the assistance of Professor V. Kibens, who showed us how to design the circuit. The circuit was designed to produce an output pulse when the input signal, the velocity at the sublayer edge u_w, reached a certain level (which could be adjusted) with either positive or negative slope with respect

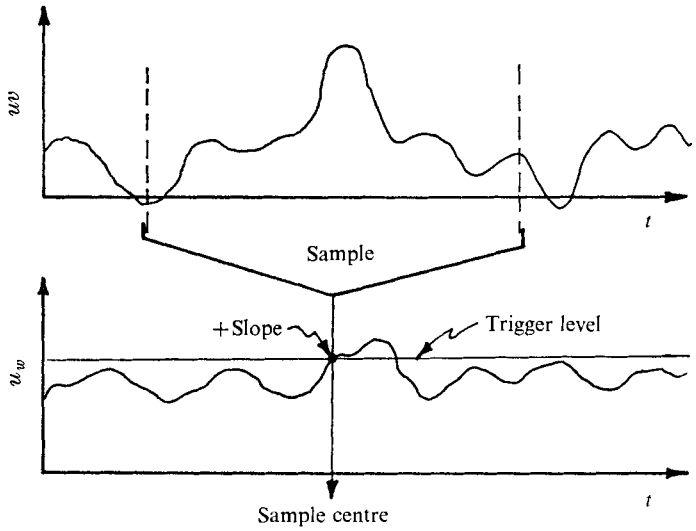

FIGURE 3. Sketch of conditional sampling method.

to time. The stored samples in the wave form eductor were plotted out on a Mosley x–y plotter.

Figure 3 is a sketch of the scheme for the conditional sampling. The trigger level circuit produces a pulse which activates a single sampling cycle of the wave form eductor. The wave form eductor consists of a bank of 100 capacitors with appropriate switching transistors that sequentially store samples of the Reynolds stress signal uv. Figure 3 is a simplified version of the actual procedure. The triggering signal in figure 3 occurs too late (in the middle of the desired sample) if the Reynolds stress signal uv is sent to the eductor at the same time as the triggering signal. This problem was eliminated by introducing a time advance equal to half the sampling time into the channel carrying the signal u_w, representing the velocity near the wall. This was accomplished with a movable playback head on the RF-1100 tape recorder.

Numerous samples of Reynolds stress data were required to obtain stable average values. We did completely reduce the data from a single high-speed run, however, it required a great deal of time and careful work owing to the long averaging time required by the wave form eductor. So much time was required for this single run (about two man-weeks of continuous running of the tape recorder) that the magnetic tape finally began to wear out. If the data had been reduced on line without a tape recorder the wind tunnel running charge would have been prohibitive. Further details about the analog data reduction process are given in the next section, where the actual experimental measurements are discussed.

We were forced to find a better way to reduce the data. We decided to use the large IBM 360/67 digital computer at The University of Michigan. To obtain efficient usage of the computer, it was necessary to convert the analog data to digital form and record it on magnetic tape. The only analog-to-digital converter available for our use was a Redcor Model 632 A/D Converter which was a part

of a Control Data Corporation Model 160A digital computer which controlled a Control Data Corporation Model 164 digital magnetic tape system. The A/D converter and multiplexer could operate with three- or four-channel input at a rate of 1000 conversions per second for each channel. This conversion rate was deemed adequate for a 100 Hz signal (i.e. one would have ten data points per cycle). It was therefore necessary to reduce the speed of the magnetic tape recorder when playing back data. The speed was reduced by a factor of eight by recording data at 60 in./s and playing back at 7·5 in./s. In this way, our digitized data were accurate to frequencies of the order of 1000 Hz. Fortunately, the signals from the hot wires in the low-speed ($U_\infty = 20$ ft/s) boundary layer contain very little energy above 1000 Hz. After the raw data had been converted to digital form, the rest of the data reduction – including plotting in some cases – was done by the IBM 360/67 computer using simple FORTRAN programs.

Further details of the data reduction are given later when the experiments are discussed. We should like to point out at this time that digital data reduction for conditional sampling measurements has definite advantages over analog sampling methods using capacitor storage devices. The advantage takes the form of flexibility in that various operations like comparison of signals, integration over short intervals, single samples or samples of clipped (i.e. truncated signals) are very simple to program. Another very important advantage is that less raw data is required to obtain stable averages because none of the data is lost or used to charge up capacitors as in the wave form eductor, where each capacitor starts out with zero charge and is provided with a finite 'leak' or time constant. It turned out that the amount of raw data required to obtain stable averages of digital data was about one-twentieth of the amount required using analog methods.

3. Experimental measurements

The measurements described below were made over a considerable period. For example, the velocity measurements at the wall using a ladder array of hot-wires were made in 1968 by Dr Bo Jang Tu in the high-speed boundary layer, as were the measurements of $\overline{u_w \omega_x}$, which were made at approximately the same time. During 1970, we made most of the measurements in the low-speed boundary layer.

3.1. *Measurements of the velocity in the sublayer*

The instantaneous streamwise velocity distribution in the sublayer was measured using four hot wires arranged in a 'ladder' array as shown in figure 4. The hot-wire array was constructed by Dr Bo Jang Tu. The signals from each wire were produced with a Miller constant-temperature hot-wire set and were then linearized. The wires were calibrated *in situ* using the measured mean velocity profile and the measured distance of the hot wires from the wall. It may be noted that the wires are rather long, stretching to about $z^+ = 265$, when immersed in the sublayer of the high-speed boundary layer. The streaks of low-speed fluid in the sublayer at low Reynolds number reported by Kline *et al* (1967) had a spanwise separation of $z^+ \simeq 100$.

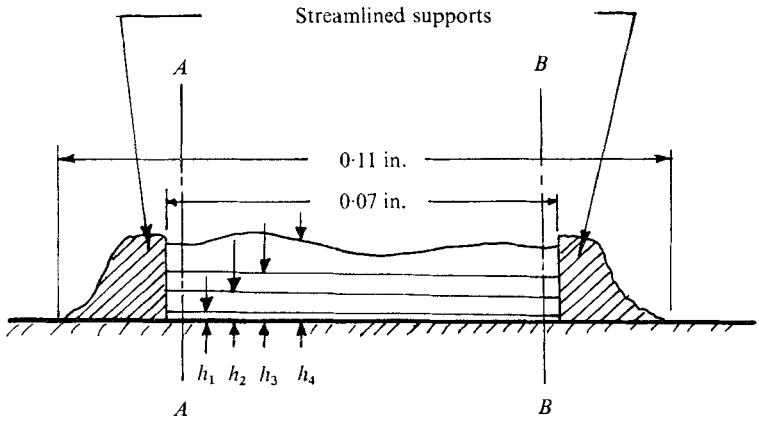

FIGURE 4. Downstream view of 'ladder' array of four hot wires for sublayer velocity measurements. $1{\cdot}5 \times 10^{-4}$ in. diameter platinum wires were used. At station A–A: $h_1 = 1{\cdot}4 \times 10^{-3}$, $h_2 = 5{\cdot}5 \times 10^{-3}$, $h_3 = 8{\cdot}8 \times 10^{-3}$, $h_4 = 13{\cdot}4 \times 10^{-3}$ in. At station B–B: $h_1 = 0{\cdot}9 \times 10^{-3}$, $h_2 = 4{\cdot}4 \times 10^{-3}$, $h_3 = 7{\cdot}9 \times 10^{-3}$, $h_4 = 13{\cdot}4 \times 10^{-3}$ in.

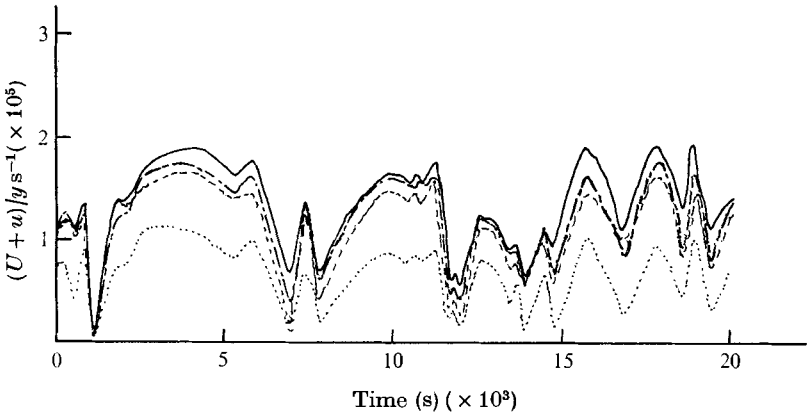

FIGURE 5. Velocity fluctuations measured in sublayer using 'ladder' array of figure 4. Miller hot-wire anemometers with linearization were used for these measurements. ——, wire 1; – – –, wire 2; — – — – —, wire 3; - - - -, wire 4. $U_\infty = 153$ ft/s.

The data obtained from the wires, see figure 5, show that the large-scale streamwise velocity fluctuations that occur in the sublayer can be thought of as a time-varying mean shear. In other words the streamwise velocity above a given point on the wall can be represented approximately by

$$u_w = \text{constant} \times yf(t). \tag{1}$$

There are obviously transverse and vertical velocity fluctuations occurring also in and near the sublayer; however, these are of much smaller magnitude. For example, the root-mean-square fluctuating velocity u' (here and elsewhere in this paper a prime denotes a root-mean-square value) is about three times and six times as large as w' and v', respectively, at $y^+ = 10$. As one approaches the wall, the ratio v'/y approaches zero, and u'/U, u'/y and w'/y are approximately

constant, see Laufer (1954).† This means that the transverse velocity field arising from the streamwise vorticity responsible for the low-speed streaks observed by Kline *et al.* (1967) and Kim *et al.* (1968) in the sublayer must be considerably less energetic than the streamwise velocity fluctuations. The primary result of our measurements of streamwise velocity is that the large-scale energetic fluctuating streamwise velocity in the sublayer $y^+ < 5$ varies approximately linearly with distance from the wall. Therefore, a single wire at $y^+ < 5$ can be used to deduce the large-scale streamwise fluctuating velocity field all the way to the wall. Note that the above measurements were made at high Reynolds number, when the sublayer is very thin: $R_\theta = 38\,000$. Similar measurements were not made at the lower Reynolds number $R_\theta = 4230$. However, there should be no qualitative difference in the primary result that the large-scale fluctuating streamwise velocity at any instant varies approximately linearly with distance from the wall.

3.2. *General considerations about the conditionally sampled measurements of Reynolds stress*

We were introduced to the concepts and methods of conditional sampling (using analog methods) by V. Kibens. (See Kovasznay, Kibens & Blackwelder (1970) for an explanation of various concepts and methods that they developed.) Our first conditionally sampled measurements of Reynolds stress were made in the high-speed boundary layer, where $R_\theta = 38\,000$, using analog methods and a wave form eductor as described in § 2. As was explained in § 2, the data averaging process during the analog sampling measurements was very time-consuming. The first measurements were exploratory in nature, but will be reported below (see § 3.2.3). We found that the measurements were possible but the spatial resolution of the flow field near the wall was poor because the sublayer thickness was very small; $y^+ = 7{\cdot}5$ corresponded to $y = 0{\cdot}002$ in. For this reason, we altered the experiment and used a lower stream speed (approximately 20 ft/s) to reduce the friction velocity and thus increase the sublayer thickness. The distance between test section entrance and measuring station was approximately 35 ft. This gave a thick turbulent boundary layer of approximately the same thickness as at high speed but with a much thicker sublayer, at $y^+ = 7{\cdot}5$, i.e. $y = 0{\cdot}019$ in. (see also table 1 and figure 1).

Another change in the experiment was the use of a large digital computer to perform the conditionally sampled measurements. The details of the hardware have been discussed in § 2. The program for conditional sampling was simple in concept. A block of digitized data from the velocity u_w near the wall, and from the velocity components u_{1n} and u_{2n} at the two wires on the X-probe (see figure 2) was read into the computer memory from the magnetic tape. The computer then compared each digitized value of the velocity near the wall with the desired constant level of the velocity u_w representing the sampling criteria. This level is proportional to the trigger level, labelled T, on the plots. When the value u_w/u'_w was equal to T, within a certain small error, the computer was told to store the product of the sum and difference of u_{1n} and u_{2n} for each digitized data point in a certain time interval before and after the sampling criteria were met. The

† Also Coantic (1965) has deduced that $u'/y \simeq 4w'/y$ near the wall.

comparison of u_w/u'_w with T was done by requiring the computer to detect the change in sign of the difference, $u_w/u'_w - T$. Note that the sign of the slope† of u_w can also be determined from the change in sign of the difference, $u_w/u'_w - T$; this was also part of the sampling procedure.

The sampled data were digitized samples of the product uv, where for two crossed wires at 90°, see figure 2,

$$uv = [(u_{1n} + u_{2n})/\sqrt{2}]\,[(u_{1n} - u_{2n})/\sqrt{2}] = \tfrac{1}{2}(u_{1n}^2 - u_{2n}^2). \tag{2}$$

It should be noted that the product uv represents only turbulent transport across a line y = constant of streamwise momentum fluctuations. Thus, uv is not the entire fluctuating stress caused by turbulence on a surface y = constant because the mean streamwise momentum is also transported by v fluctuations and the mean velocity V in the y direction also transports fluctuations in streamwise momentum. The true fluctuating stress is $(U+u)(V+v) - UV$. We are indebted to S. Corrsin for reminding us of this fact. In the boundary layer $V = O(U_\infty \delta/L)$, so that the most important terms in the fluctuating stress are Uv and uv. We have not studied the term Uv in detail. A few measurements show that contributions from this term are appreciable but the interpretation becomes quite complicated, and a discussion of these results will be included in a report at a later date. For the present, we shall confine our discussion to the term uv, which is the only term ultimately contributing to the average of the fluctuating stress, i.e., the Reynolds stress = $\overline{uv}$.

Returning to the discussion of the computerized data reduction process, we found that to avoid excessive computing time and expense it was necessary to read the data from the tape into the computer as infrequently as possible. Therefore, the program was designed to perform the conditional sampling for all values of T and for both positive and negative slope of u_w in one pass or reading of the tape. Files were set up for storage of sampled data for each trigger level and slope. After the program had been run, the stored data were plotted in final form using a CalComp plotting system. We did not use a printed digital output because the sheer mass of data was too great for efficient comprehension.

Our first analog conditionally sampled data were obtained using the full bandwidth of the signal (u_w). We found that numerous extraneous samples were obtained compared with conditionally sampled data obtained when high frequencies were removed from the signal u_w. We therefore sampled the low-speed measurements of the Reynolds stress using both filtered and unfiltered u_w signals. The analog filter was a low-pass Butterworth filter of third order with half-power point at 10 Hz. The filter was constructed using an Applied Dynamics PB-64 Analog Computer. The signal u_w was filtered before the recorded analog data were digitized. Since the analog data were played back from magnetic tape at $\frac{1}{8}$ the recording speed before A/D conversion, the filter half-power point was actually 80 Hz in real time.

3.2.1. *Conditionally sampled measurements of Reynolds stress at a single point near the wall.* The plots of sampled data that we obtained are very numerous. In order to conserve space we show in figure 6 only a few examples of plots of

† The derivative of u_w with respect to time.

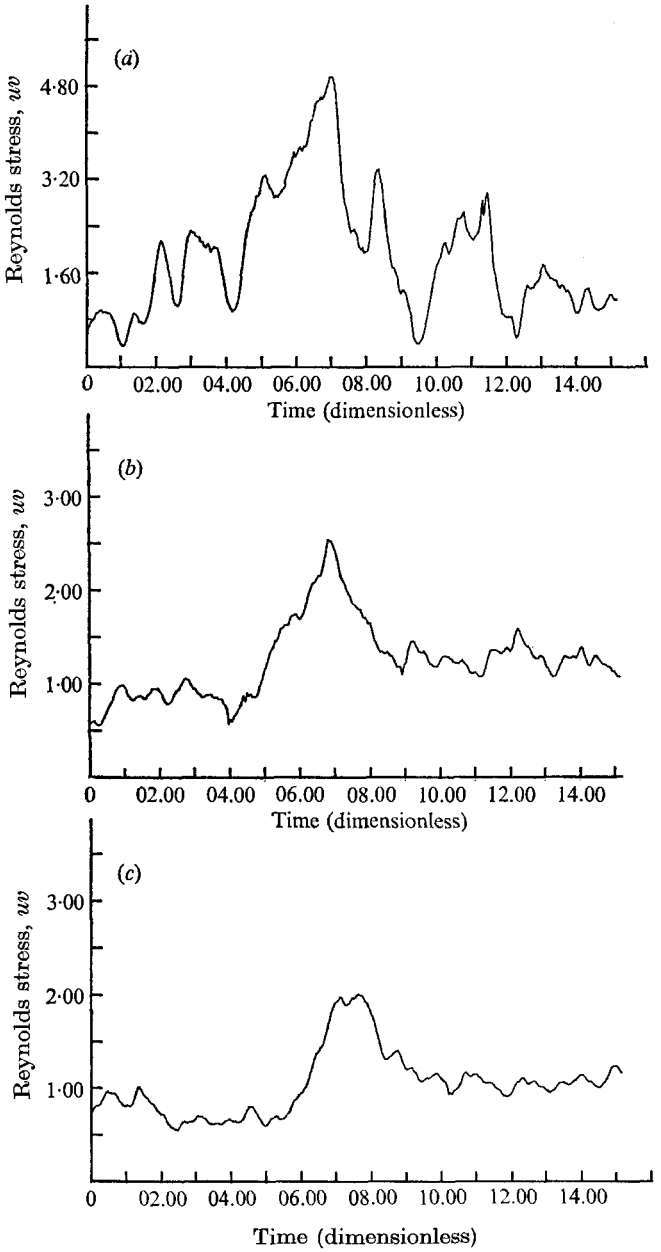

FIGURE 6 (*a–c*). For legend see p. 79.

sampled Reynolds stress for the low-speed boundary layer when the signal u_w was filtered to remove high frequencies. The hot wire producing the signal u_w is located at a distance $y = 0{\cdot}037$ in. from the wall, or $y^+ = 16{\cdot}2$. This location was chosen because of Corino & Brodkey's (1969) observation that the approximate centre of the low-speed region near the wall was at $y^+ = 15$. The data of figure 6 show sampled contributions to $\overline{uv}$ for various trigger levels: $u_w/u'_w = \pm 2{\cdot}15$, $\pm 1{\cdot}07$, $\pm 0{\cdot}54$ and 0. The quantity uv was measured with the X-wire located

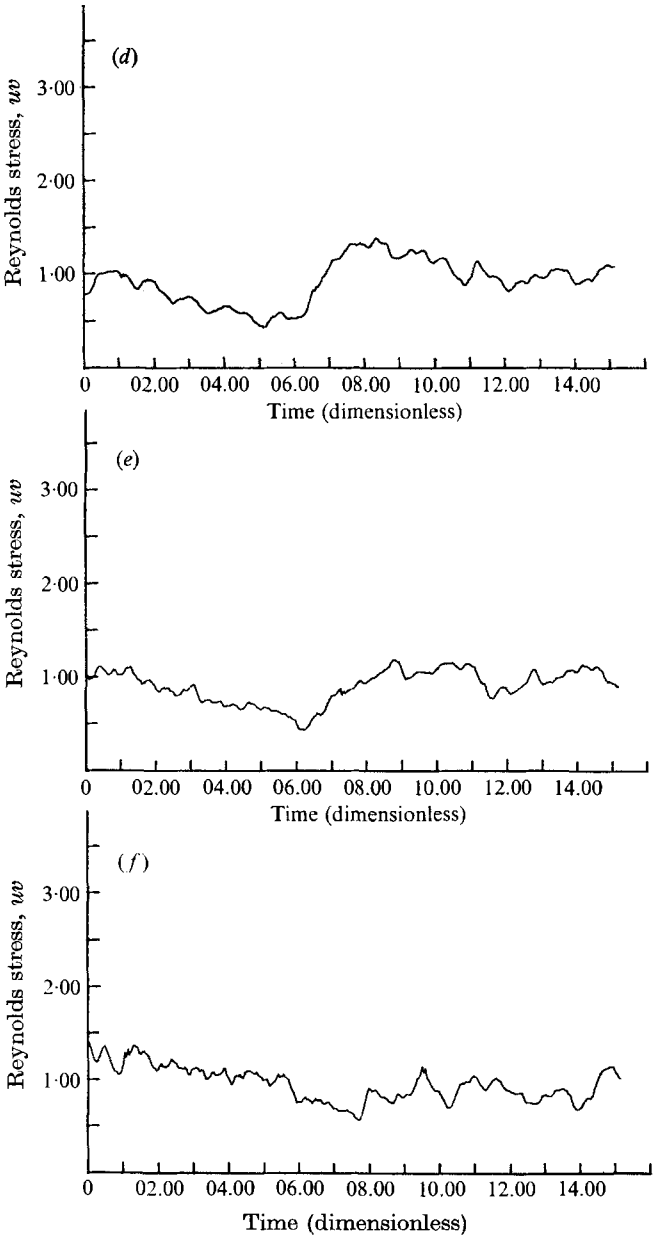

FIGURE 6 (*d–f*). For legend see p. 79.

directly above the point where u_w was measured. The centre of the X-wire was located at $y = 0{\cdot}07$ in. or $y^+ = 30$. Again, Corino & Brodkey (1969) indicate that this is the approximate location of the region of violent interaction.

In figure 6 the ordinate variable called Reynolds stress, uv, is the ratio of the average value of the samples of uv to the overall average value of uv, i.e. $\overline{uv}$. Thus, the ordinate variable is

$$\text{Reynolds stress, } uv = 1/N \sum_{i=1}^{N} (uv)_i / \overline{uv} = \widetilde{uv}/\overline{uv}, \tag{3}$$

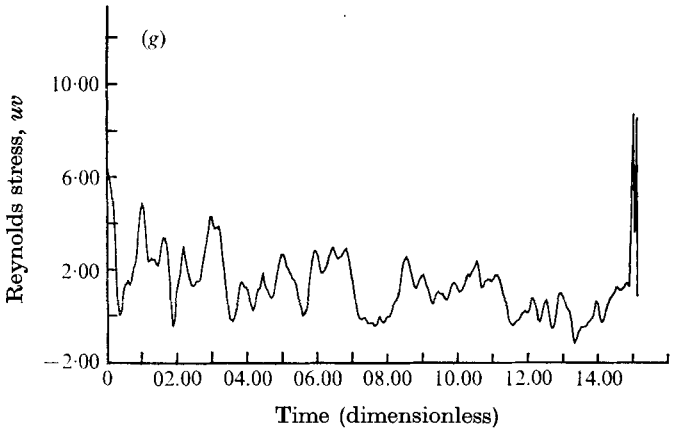

FIGURE 6. Conditionally sampled measurements of contributions to the Reynolds stress (see text for definition of abscissa variable, ordinate variable and T). Each plot is for negative slope. (*a*) $T = -2{\cdot}5$, $n = 38$, (*b*) $T = -1{\cdot}07$, $n = 514$, (*c*) $T = -0{\cdot}54$, $n = 916$, (*d*) $T = 0$, $n = 1132$, (*e*) $T = 0{\cdot}54$, $n = 929$, (*f*) $T = 1{\cdot}07$, $n = 465$, (*g*) $T = 2{\cdot}15$, $n = 7$, where n is the number of samples of uv obtained at each value of T.

where n is the number of stored samples that have accumulated in each storage file when the data reduction is complete. The abscissa variable of the plots in figure 6 called time (dimensionless) is the dimensionless time tU_∞/δ^*, time being zero at the beginning of the sample. Note that the sampling criteria $u_w/u'_w = T$ with negative slope occurs in figure 6 at the midpoint of the sampled data.

Finally, one should note that in figure 6, see (3), the ratio $\widetilde{uv}/\overline{uv}$ should be one if the N samples are selected at random times or if the sampling criteria are unrelated to the data that is being sampled. Accordingly, it is clear that the large significant contributions to $\overline{uv}$, $\widetilde{uv} \simeq 5\,\overline{uv}$ are made with $T = -2{\cdot}15$ (see figure 6(*a*)) at dimensionless time $tU_\infty/\delta^* = 7{\cdot}0$; at $T = 0$ (figure 6(*d*)) the contribution is $\widetilde{uv} \simeq 1{\cdot}4\,\overline{uv}$ at the centre of the interval. For positive T, the contribution to $\overline{uv}$ is somewhat less than one at the centre of the sampling interval, see figures 6(*e*)–(*g*).

The data of figure 6 are typical of all the sampled data for uv that we have collected except that the data of figure 6 show the largest values of $\widetilde{uv}$ because the sampling criteria have been improved by filtering out high frequency noise from the signal u_w.

We shall now consider how one can obtain a quantitative assessment of the total contribution of $\widetilde{uv}$ to $\overline{uv}$ as a function of T. The data of figure 6 do not contain enough information to assess the relative contribution made by $\widetilde{uv}$ at each T. We need information about the frequency of occurrence, or the relative number, of samples obtained at each T. This information can be obtained from the probability density of the signal u_w. A program was written to generate an indicator function $\phi(T;t)$ for many closely spaced values of T. Here the indicator function (see Lumley 1970 for a complete explanation) is defined as

$$\phi(T;t) = \begin{cases} 1 & u_w/u'_w < T, \\ 0 & u_w/u'_w \geqslant T. \end{cases} \tag{4}$$

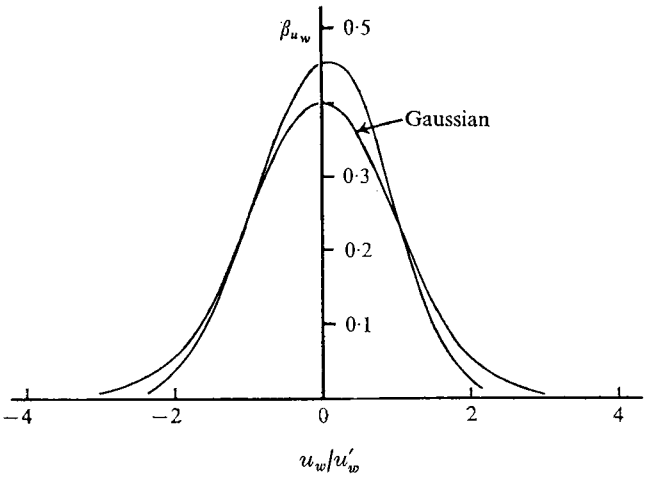

FIGURE 7. Probability density of u_w after passing the signal u_w through a low-pass Butterworth filter at third order with half-power point at 80 Hz. The velocity u_w was measured at $y^+ = 16{\cdot}2$ and the stream speed was 19·7 ft/s.

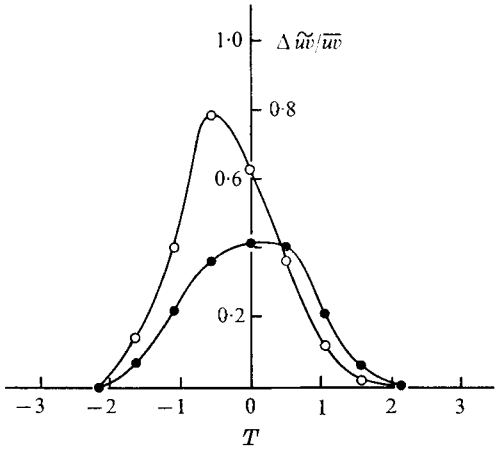

FIGURE 8. Conditionally sampled contributions to $\overline{uv}$ as a function of T. A low-pass filter was used for u_w, with frequency band $0{\cdot}26 < f < 80$ Hz. The signal uv was sampled when $u_w = Tu'_w$, X-wire location $x^+ = 0$, $y^+ = 30$; $U_\infty = 19{\cdot}7$ ft/s. ○, negative slope; ●, positive slope.

From time averages of the indicator function, the probability distribution of u_w was obtained. By differentiation with respect to u_w, β_{u_w}, the probability density of u_w, was obtained and is shown in figure 7. The probability density for a Gaussian distribution is also shown in figure 7 for reference.

With the data of figure 7 at hand, one can now obtain a qualitative measure of the contribution of $\widetilde{uv}$ to $\overline{uv}$ as a function of T. This measure is obtained by multiplying the value of $\widetilde{uv}/\overline{uv}$, at the time the triggering criteria $u_w/u'_w = T$ was met, by the probability density at that T. The result is shown in figure 8. The ordinate variable in figure 8, $\Delta\widetilde{uv}/\overline{uv}$, is given by

$$\Delta\widetilde{uv}/\overline{uv} = \widetilde{uv}/\overline{uv}\,\beta_{u_w}. \tag{5}$$

Note that the integral,

$$\frac{1}{2}\int_{-\infty}^{\infty}[(\Delta\widetilde{uv}/\overline{uv})_{-}+(\Delta\widetilde{uv}/\overline{uv})_{+}]\,dT = 1, \tag{6}$$

where the subscripts $\pm$ refer to the sign of the slope, so that the ordinate variable in figure 8 is a measure of the contribution per unit T of sampled uv data to the value of $\overline{uv}$. The ordinate variable (5) for negative slope is not symmetric about the origin $T = 0$ and has a maximum value at $T \simeq -0{\cdot}7$. The data for positive slope are also shown in figure 8 and are much more symmetrical about the origin $T = 0$. This indicates that greater contributions to Reynolds stress occur when the velocity near the wall is less than the mean value and decreasing. This result adds additional information to what is known from the visual studies of Kim *et al.* (1968) and Corino & Brodkey (1969). In the visual studies the velocity at the wall was not measured but it was determined by both the above groups of authors that u_w was low during bursting. Kim *et al.* also state that the velocity profile was inflexional. We can now add that, from the present data, the bursts occur when the velocity profile first becomes inflexional, i.e. when the wall velocity is low and decreasing. It will be recalled, from the result of figure 5, that when the sublayer velocity decreases at a given point it also decreases at every point in the sublayer above or below the given point, the decrease being proportional to distance from the wall. In addition, in a recent study Blackwelder & Kaplan (1971) have made conditionally sampled measurements of the streamwise velocity profile for $2 < y^+ < 80$ when the streamwise velocity at $y^+ = 15$ indicates that intense small-scale turbulence is present at that point. Their results show that the velocity profile is inflexional near the wall when bursts occur at $y^+ = 15$.†

When the slope of u_w is positive, a low value of u_w is not related to unusually large contributions, at that time, to $\overline{uv}$. As a matter of fact, the conditionally sampled data for positive slope (analogous to the data of figure 6) show that for $T < 0$ unusually large contributions to $\overline{uv}$ are made *but at times prior* to the time when $u_w/u'_w = T$ with positive slope. This indicates that when $u_w/u'_w = T$ with positive slope the burst has already occurred (when $u_w/u'_w = T$ with negative slope) and now when u_w is increasing the bursting event is over.

Figure 9 shows the contributions to the Reynolds stress from samples of the signal uv that are obtained at various values T of the unfiltered velocity near the wall. The results of figure 9 should be compared with those of figure 8. Note that in figure 9 the curve for negative slope is again unsymmetrical about the origin $T = 0$ but the difference between the curves for positive and negative slope is much smaller than in figure 8. This shows that the filtered signal u_w provides better criteria for the identification of samples of uv that contribute to the Reynolds stress when u_w decreases. We should also emphasize the fact that in the digital data reduction program a sample of uv was taken whenever $u_w/u'_w = T$. Therefore, if u_w had many rapid changes in value while a burst was occurring the

† After this paper was written Grass (1971) reported conditionally sampled hydrogen-bubble flow visualization measurements of velocity profiles and Reynolds stress throughout the boundary layer. His results agree with ours and add valuable information about the flow throughout the boundary layer.

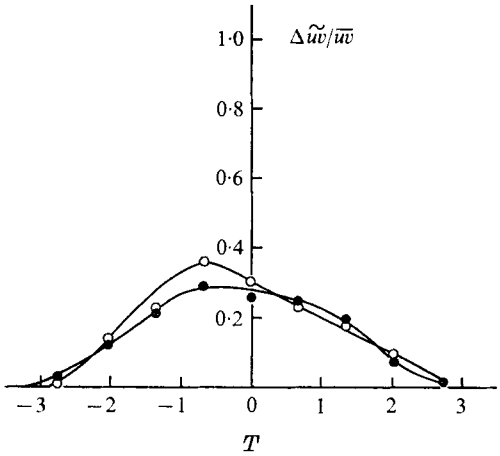

FIGURE 9. Conditionally sampled contributions to $\overline{uv}$ as a function of T. Frequency band for u_w was $0{\cdot}26 < f < 8000$ Hz. The signal uv was sampled when $u_w = Tu'_w$, X-wire location $x^+ = 0$, $y^+ = 30$; $U_\infty = 19{\cdot}7$ ft/s.

signal u_w might pass through the trigger level more than once during the burst. This would cause the same burst in uv to be stored on top of itself but shifted in time. Therefore, the large contributions to $\widetilde{uv}$ would in effect be smeared out and reduced over the sampling interval.

3.2.2. *Spatial distribution and decay of sampled Reynolds stress.* We have made conditionally sampled measurements of Reynolds stress at various distances from the wall when the X-wire is at various locations transverse and downstream from the u_w wire, which is located at the point $y^+ = 16{\cdot}2$. The results of these measurements have not yet been fully analysed. However, we can state that the measurements show that the largest contributions to $\overline{uv}$ from the sampled signal uv occur when $u_w < 0$ with negative slope and are confined to a narrow (in the spanwise direction) region near the wall and downstream of the u_w wire. The approximate dimensions of the narrow region are $x < 2{\cdot}5$ in., $y < 0{\cdot}35$ in. and $z < 0{\cdot}35$ in., or $x^+ < 1110$, $y^+ < 154$ and $z^+ < 154$. There is also evidence that the spanwise extent of the region in which appreciable contributions to the sampled Reynolds stress occur increases in width downstream of the point where u_w is measured. For example, no contribution, $\widetilde{uv}/\overline{uv} = 1$, was obtained at $x = 0{\cdot}2$ in., $y = 0{\cdot}07$ in., $z = 0{\cdot}08$ in., but an appreciable contribution was obtained at $x = 0{\cdot}5$ in., $y = 0{\cdot}08$ in., $z = 0{\cdot}1$ in. The angle θ, between the stream direction and edge of the region of contributions to $\overline{uv}$ (i.e. $\widetilde{uv} > \overline{uv}$), is therefore in the range $12° < \theta < 23{\cdot}5°$. The disturbance is also convected downstream. An approximate convection velocity was measured from the change in the location (in time) of the maximum contribution from the conditional samples $\widetilde{uv}$ (for $T < 0$ with negative slope) at a succession of points downstream of the point where u_w was measured. The convection velocity was approximately the local mean speed at the distance from the wall where uv was measured.

3.2.3. *Effect of Reynolds number on conditionally sampled Reynolds stress measurements.* We have not yet investigated in any detail the contributions to $\overline{uv}$ from sampled measurements of uv at high Reynolds number. We have one set of

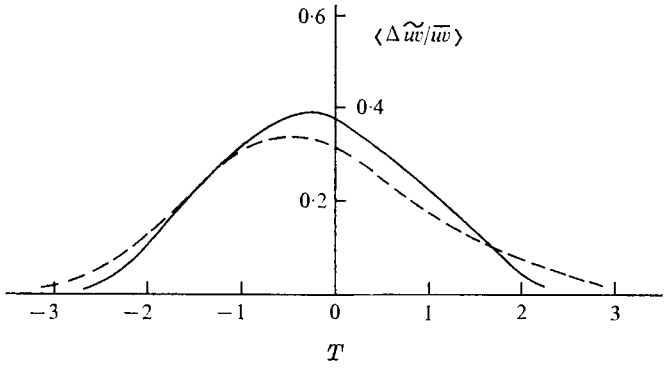

FIGURE 10. Average of sampled contributions to uv for positive and negative slope as a function of T at low and high Reynolds number. No filter was used for u_w. Hot-wire locations were: $y^+ = 7{\cdot}5$ for u_w measurements, $x^+ = 1690$, $y^+ = 263$ for uv measurements for high Re; $y^+ = 8{\cdot}3$ for u_w, $x^+ = 762$, $y^+ = 116$ for uv for low Re. ——, $R_\theta = 38000$; – – – –, $R_\theta = 4700$.

measurements made at $R_\theta = 38000$ with analog data reduction. The signal u_w was not filtered to remove extraneous high frequency signals. Nevertheless, appreciable contributions to $\overline{uv}$ were made near the wall when u_w was negative and decreasing. The measurements are in qualitative agreement with the results already described in § 3.2.1 (see figure 9) for a boundary layer at lower Reynolds number $R_\theta = 4230$. The results of the low and high Reynolds number measurements at points downstream from the point where u_w was measured are shown in figure 10. The ordinate variable in figure 10 is

$$\langle \Delta \widetilde{uv}/\overline{uv} \rangle = \tfrac{1}{2}[(\widetilde{uv}/\overline{uv})_+ + (\widetilde{uv}/\overline{uv})_-]\beta_{u_w}, \tag{7}$$

which is the average of the contribution from uv for positive and negative slope. As noted in (6), the area under each curve in figure 10 should be unity. From the similarity between these two sets of data at widely different Reynolds number and points which correspond, within a factor of 2·5, in wall variables x^+, y^+ and z^+ we can conclude that the burst phenomena still occur when $u_w < 0$ at high R_θ. Note that from the area under each curve for $T < 0$ we can state that 60 % of the Reynolds stress at the given downstream locations is produced when the upstream velocity near the wall is lower than the mean. We add that for the data in figure 10 the hot wire near the wall is located at $y = 0{\cdot}002$ in., or $y^+ = 7{\cdot}5$, for $R_\theta = 38000$ and at $y = 0{\cdot}019$ in., or $y^+ = 8{\cdot}3$, for $R_\theta = 4230$. This location is nearer the wall than those used for the data of figures 8 and 9.

3.2.4. *Conditionally sampled Reynolds stress measurements with an improved detection scheme.* The use of a low-pass filter for the signal u_w resulted in improved detection of contributions to $\overline{uv}$. We then realized that still greater improvement in our detection criteria might result if we used a crude spanwise spatial filter for the detector signal u_w. To accomplish this, we installed two hot wires side by side at $y = 0{\cdot}037$ in., or $y^+ = 16{\cdot}3$. The wire length was $l = 0{\cdot}045$ in. or $l^+ = 20$. The wires were soldered onto the tips of three needles at the same streamwise station. The central needle was common to both wires. The distance between the centres of the wires was therefore $l = 0{\cdot}045$ in., or $l^+ = 20$. This distance is

approximately one-fifth of the wavelength of the low-speed streak structure observed in the sublayer by Kline *et al.* (1967).

The sampling criteria which we used with the two velocity signals u_{w_1} and u_{w_2} from the wires side by side near the wall was based on the idea that, if a burst event occurred directly above them, both u_{w_1} and u_{w_2} would be decreasing and less than the mean. In other words, the plane between the two wires that is normal to the wall and is parallel to the free stream would be a plane of symmetry for the burst event if $u_{w_1} = u_{w_2}$ when both decreased.

We digitized four channels of data obtained at $U_\infty = 20$ ft/s with the X-wire slightly downstream from and centred between the wires producing the signals u_{w_1} and u_{w_2}. The X-wire was located at $y = 0{\cdot}07$ in. from the wall (or $y^+ = 30{\cdot}5$) and was $x = 0{\cdot}18$ in. (or $x^+ = 78{\cdot}5$) downstream from the wires for u_{w_1} and u_{w_2}. Upon examining the data, we could observe that there were a number of occasions when, for negative T, $u_{w_1}/u_1' < T$ with negative slope at the same time that $u_{w_2}/u_2' < T$ with negative slope. However, in many instances, even when high frequencies were removed from both u_{w_1} and u_{w_2} (as was described in § 3.2.1), the two signals did not both remain less than T for the same length of time. It was clear that some kind of integral condition over time had to be added to the sampling criteria. This was accomplished by writing a computer program that summed all the digitized data values for u_{w_1} and u_{w_2} during the time that both signals were below a specified negative trigger level, provided that both signals simultaneously (within a small error) fell below the specified trigger level. The sums of digitized data values for both u_{w_1} and u_{w_2} were then compared and if the sums were both greater in magnitude than a specified value, and if both the signals u_{w_1} and u_{w_2} simultaneously (within a small error) rose above the specified trigger level, a burst event was presumed to have occurred. In operation, the program caused the computer to search the digitized data recorded on magnetic tape for special events meeting the above criteria. As one might perhaps expect, events meeting the above criteria were not numerous. In 52 seconds of data or $4{\cdot}1 \times 10^5$ digitized data points we found only ten events meeting the above criteria.

For each event the computer then plotted the signal uv. In each case when $T = -1$ (i.e. $u_{w_1} = u_{w_2} = -u_w'$) and the slope of u_w was negative, large contributions to $\overline{uv}$ ($uv > 20\,\overline{uv}$) occurred at some time within the sampling interval, which included 300 digitized data points or was 0·0375 s in duration. In some samples a number of contributions occurred, each of the order of 10–$20\,\overline{uv}$. In other samples, single or double contributions which were twice as large occurred. In one case, two large contributions, $uv \simeq 60\,\overline{uv}$, occurred. An example of a single large contribution to $\overline{uv}$ is shown in figure 11. The contribution is $uv = 62\,\overline{uv}$ at the peak. These results represent truly sizeable contributions to the Reynolds stress during bursting events. This is qualitatively in accord with the results and conclusions of Kim *et al.* (1968) and Corino & Brodkey (1969). However, neither of the above sets of authors could accurately measure the magnitude of the contributions to $\overline{uv}$ during a burst, but both agreed that the bursting events were very energetic. We have also applied the above specialized detection criteria to our data for positive T ($T = 1{\cdot}0$) with positive slope in an attempt to observe the sweep event described by Corino & Brodkey (1969). Recall from the introduction that the

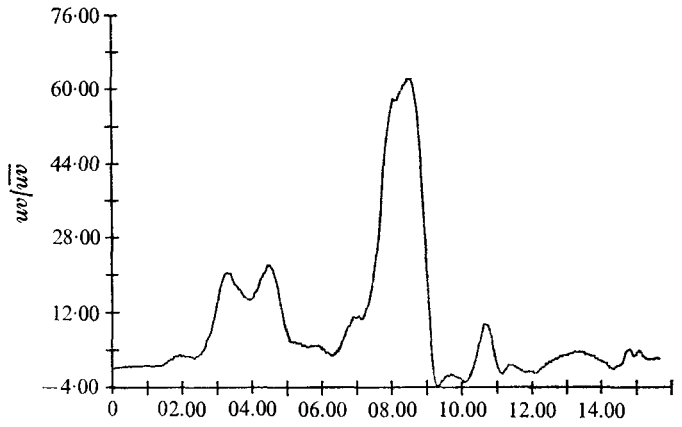

FIGURE 11. Example of a very large single contribution to Reynolds stress. Sample found using special spatial and temporal filtering criteria, see § 3.2.4. Slope is negative, $T \simeq -1{\cdot}00$, $n = 1$. Abscissa variable the same as in figure 6.

sweep was observed after the burst when higher speed fluid enters the field of view. We found approximately 12 events meeting the detection criteria and in all these events appreciable contributions to $\overline{uv}$ occurred. The signal uv was not as peaked as it was during bursting, but appeared to be relatively constant and large, $uv \simeq 7\,\overline{uv}$, for longer times than during bursting. This was our first strong indication that not all the contributions to Reynolds stress near the wall are associated with outflow of low-speed fluid. Note that Kim *et al.* (1968) state that essentially all the contributions to $\overline{uv}$ occur during bursting. Corino & Brodkey estimate that 70 % of the average contribution to $\overline{uv}$ occurs during bursting.

3.3. *Streamwise vorticity measurements*

As was mentioned earlier, we have also made measurements of streamwise vorticity fluctuations ω_x, and found that the streamwise vorticity fluctuations near the wall are correlated with the velocity u_w at the edge of the sublayer. The measurements were made by Dr Bo Jang Tu and the senior author in 1968 in the high-speed boundary layer. The correlation coefficient between u_w and ω_x,

$$R_{u_w\omega_x} = \overline{u_w\omega_x}/u'_w\omega'_x, \tag{8}$$

was found to be a maximum along a highly swept back line passing through the point on the wall where u_w is measured and proceeding downstream and away from the wall at an angle to the wall and to the stream of approximately 10°. The maximum correlation coefficient that was measured was $R_{u_w\omega_x} = -0{\cdot}095$. The vorticity probe was really much too large (wire spacing $l^+ \simeq 250$) for correct measurements of the small-scale eruption phenomena. These results give only a qualitative description of the eruption process. The arrangement of the vorticity probe for the above measurement is shown in figure 12. The location of the probe when maximum negative correlation was found is shown in figure 12, where the distances are $x = 1{\cdot}0$ in. (or $x^+ = 1250$), $y = 0{\cdot}149$ (or $y^+ = 185$) and $z = 0{\cdot}203$ (or $z^+ = 250$) relative to the upstream point where u_w was measured.

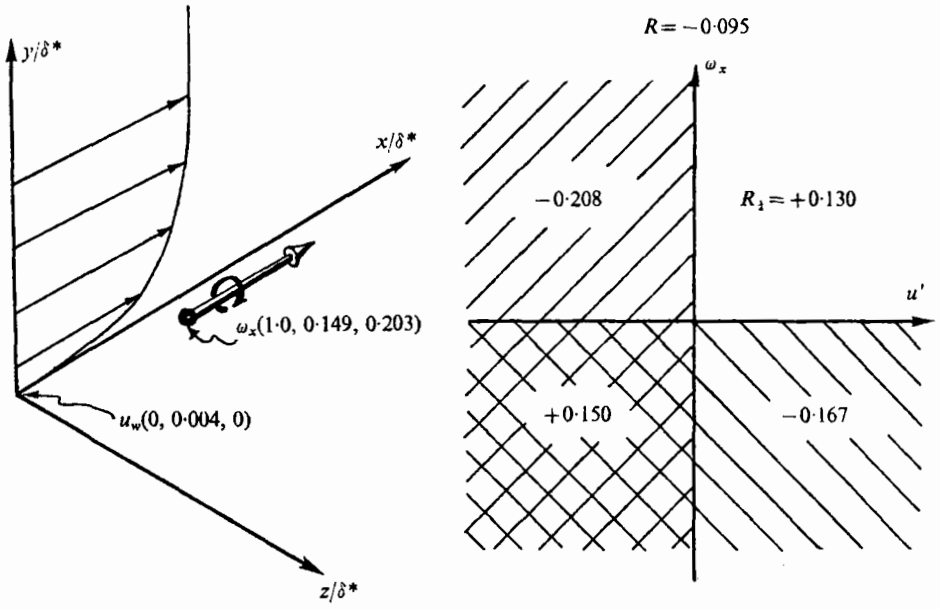

FIGURE 12. Contributions to correlation between streamwise vorticity and velocity in the sublayer from four quadrants in the u, ω_x plane. $U_\infty = 204$ ft/s. Note, $R_{\frac{1}{4}} = 1/2\pi = 0{\cdot}159$ for two uncorrelated Gaussian random variables.

We have measured the contributions to the correlation $R_{u_w\omega_x}$ in four quadrants of the u_w, ω_x plane; the results are displayed in figure 12. Note that the bulk of the negative correlation occurs in the second quadrant $u_w < 0$, $\omega_x > 0$. Here the correlation in the first quadrant (for example) is simply given by (8), but with $u_w > 0$, $\omega_x > 0$ in the numerator only. The quarter correlation was measured using an analog method (a diode in the feedback loop of an operation amplifier). The results of figure 12 show that, when $u_w < 0$, positive values of ω_x are more likely than negative values. This suggests that the positive streamwise vorticity component is associated with the burst phenomena which occurs when $u_w < 0$.

To examine this possibility in more detail, we made conditionally sampled measurements of ω_x for the above data. The results of the measurements show that when u_w passes below a given negative value (with negative slope) the sampled data for ω_x were positive for $z > 0$ and were negative when $z < 0$. These sampled contributions were appreciable. We can therefore conclude that during a burst event there is an appreciable antisymmetric pattern of streamwise vorticity present in the region near the wall centred at the point where u_w is measured. Note that the positive sign of the vorticity component ω_x at the probe location shown in figure 12 is consistent with upwelling of low-speed fluid from the wall into the outer flow downstream of the point where u_w is measured.

The sampled data for ω_x representing contributions to $\overline{\omega_x} = 0$ when $u_w > 0$ with positive slope were all negative. This result may be consistent with the idea that just before or during the sweep event (u_w increasing) high-speed fluid approaches the wall in a jet-like flow with a pattern of downstream vorticity whose rotation is opposite to that of the bursting pattern. Additional study of this phenomena should be undertaken.

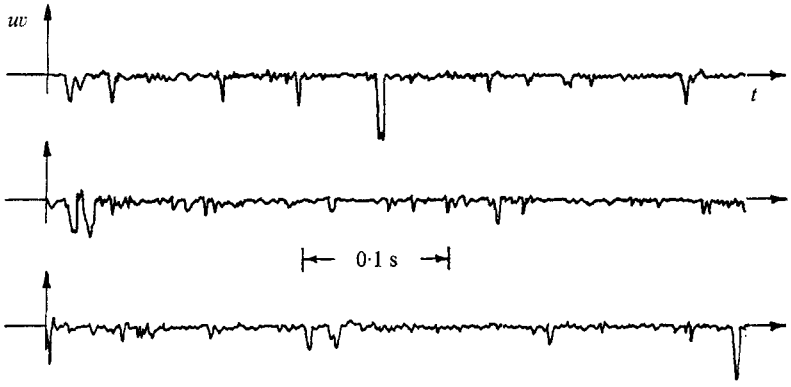

FIGURE 13. The signal uv as a function of time at $y^+ = 30$ in the low-speed boundary layer; $U_\infty = 19{\cdot}7$ ft/s.

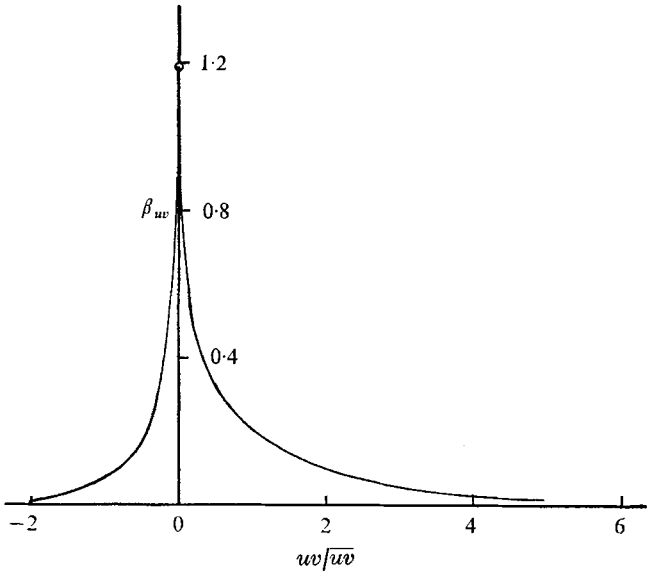

FIGURE 14. Probability density of uv measured at $y^+ = 30$ in low-speed boundary layer; $U_\infty = 19{\cdot}7$ ft/s.

3.4. *Direct observations and measurements of the signal uv and of the Reynolds stress*

The flexibility and relative simplicity of digital computation methods were exploited in a study of the signal uv from the X-hot-wire probe.

3.4.1. *Nature of the signal uv.* Figure 13 displays the signal uv as a function of time. The signal was obtained from the X-wire when it was located at a distance $y = 0{\cdot}07$ in., or $y^+ = 30{\cdot}5$, from the wall in the low-speed boundary layer, with $R_\theta = 4230$. The signal very definitely contains large short-duration negative spikes and much smaller positive contributions of considerably longer duration than the negative spikes. For a considerable fraction of the time, the signal uv is approximately zero. This suggests that the signal uv from the region in the

$u < 0, v > 0$		$u > 0, v > 0$	
Summation uv	−0·39647E 10	Summation uv	0·51697E 09
Time	36902	Time	21933
Number of samples	2555	Number of samples	3122
$\widetilde{uv}/\overline{uv}$	2·747	$\widetilde{uv}/\overline{uv}$	−0·603
% time	29·29 %	% time	17·41 %
Time/sample	14·44	Time/sample	7·03
$(\widetilde{uv}/\overline{uv})$/sample	39·68	$(\widetilde{uv}/\overline{uv})$/sample	−4·23
Fractional contribution to $\overline{uv} = 0{\cdot}805$		Fractional contribution to $\overline{uv} = -0{\cdot}105$	

$u < 0, v < 0$		$u > 0, v < 0$	
Summation uv	0·66439E 09	Summation uv	−0·21444E 10
Time	22033	Time	45132
Number of samples	2656	Number of samples	3223
$\widetilde{uv}/\overline{uv}$	−0·771	$\widetilde{uv}/\overline{uv}$	1·215
% time	17·49 %	% time	35·82 %
Time/sample	8·30	Time/sample	14·00
$(\widetilde{uv}/\overline{uv})$/sample	−6·40	$(\widetilde{uv}/\overline{uv})$/sample	17·01
Fractional contribution to $\overline{uv} = -0{\cdot}135$		Fractional contribution to $\overline{uv} = 0{\cdot}435$	

TABLE 2. Computer print-out of contributions to Reynolds stress in four quadrants of the u, v plane. The signal uv was measured at $y^+ = 30$ in the low-speed boundary layer; $U_\infty = 19{\cdot}7$ ft/s.

boundary layer where turbulent kinetic energy is a maximum is highly intermittent.

3.4.2. *Probability density of uv.* We measured the probability density β_{uv} of uv using the same computer program developed to find the probability density of u_w, see § 3.2 and equation (4). The result is shown in figure 14. Note that for this unusual random signal the maximum value of β_{uv} occurs at zero but the mean value is located at $uv/\overline{uv} = 1$, at which point $\beta_{uv} \simeq \frac{1}{6}(\beta_{uv})_{\max}$. Furthermore, the probability density has a long 'tail' for positive $uv/\overline{uv}$ and rapidly vanishing values of β_{uv} for $uv/\overline{uv} < 0$. These features† of the probability density of uv are consistent with the behaviour of uv as shown in figure 13. The peak β_{uv} at $uv = 0$ corresponds to the fact that uv is relatively quiescent or nearly zero much of the time. The long 'tail' of β_{uv} for $uv/\overline{uv} > 0$ is a result of the spiky nature of Reynolds stress contributions during bursting events.

3.4.3. *Four quadrant correlation map of contributions to* $\overline{uv}$. To obtain a quantitative measure of the intermittency of the uv signal and to better understand the nature of contributions to $\overline{uv}$ from the burst and sweep processes, we have computed contributions to $\overline{uv}$ in four quadrants of the u, v plane. The contributions of the correlation $\overline{uv}$ in each quadrant were computed for each pair of digitized data values for u and v. The product uv was added to previous values of uv in each of four storage files according to the signs of u and v. Also, a count of

† We have recently computed β_{uv} assuming that β_u and β_v are Gaussian and that $\overline{uv}/u'v' = -0{\cdot}5$. The resulting probability density distribution β_{uv} is very similar to the measurements of figure 14 with the one exception that $\beta_{uv} \to \infty$ at $uv = 0$.

the number of samples contained in each of the four storage locations was made. From these data we computed the relative contributions to $\overline{uv}$ from each quadrant, the time spent by the signal uv in each quadrant and the number of uninterrupted individual contributions to $\overline{uv}$ made by the signal uv in each quadrant. The individual contributions are called samples.

Table 2 is a copy of the computer print-out of this data reduction procedure. Note that the largest contribution to Reynolds stress, $\widetilde{uv}/\overline{uv} = 0{\cdot}805$, occurs in the quadrant $u < 0$, $v > 0$, and this represents violent upwellings of low-speed fluid. There is, however, also a large contribution (0·435) to Reynolds stress in the fourth quadrant, where $u > 0$ and $v < 0$. This contribution may be the result of the sweep event described by Corino & Brodkey (1969) or may occur as a result of the swirling motion during a burst event that has often been observed by Kim *et al.* (1968). In the swirling motion, high-speed fluid, with $u > 0$, must pass the measuring station and enter the wall region, as $v < 0$. However, during bursting u_w is lower than the mean and our data for sampled Reynolds stress in figures 8, 9 and 10 all show that considerable contributions to Reynolds stress are made when u_w is greater than the mean value. This indicates that the major contribution to Reynolds stress in the fourth quadrant $u > 0, v < 0$ *is* caused by the sweep event and *not* during bursting. This important conclusion will be discussed again below.

At approximately the same time that these measurements were made the paper by Wallace, Eckelmann & Brodkey (1972) appeared. They report similar measurements of contributions to $\overline{uv}$ in four quadrants using analog computer elements. Their measurements were made in a fully developed turbulent channel flow using oil as a working fluid. The Reynolds number based on channel width and a centre-line velocity of 19·5 cm/s was 7150. Under these conditions the sublayer ($y^+ = 7{\cdot}5$) was 0·44 cm thick. The results of their four quadrant measurements of $\overline{uv}$ contributions are in substantial agreement with ours and reveal that the major contributions occur in the second and fourth quadrants. Wallace, Eckelmann & Brodkey also made a traverse of the wall region $3 < y^+ < 180$ and found that near the wall $y^+ \simeq 15$ the contributions to $\overline{uv}$ from the second and fourth quadrants were equal. For $y^+ < 15$ the fourth quadrant (sweep event) made the largest contribution while for $y^+ > 15$ the contribution from the second quadrant (erruption) was the largest. At $y^+ = 30$ the second-quadrant contribution was only 13 % larger than the fourth-quadrant contribution. Our measurements at $y^+ = 30$ show that the second-quadrant contribution is 85 % larger than the fourth-quadrant contribution. The difference may be an effect of the higher Reynolds number of our flow or the fact that our measurements were made in a boundary layer and not in a channel flow.

3.4.4. *Four quadrant correlation maps of the contribution to $\overline{uv}$ above a certain value of $|\overline{uv}|$.* Contributions to the correlation $\overline{uv}$ were also measured in four quadrants of the u, v plane when the signal $|uv|$ was greater than a certain value of $|uv| = H$ (say). The purpose of these measurements, which were easily done by a slight alteration of the computer program, was to single out the large contributions to $\overline{uv}$ which occur in the second quadrant $u < 0, v > 0$. The program alteration consisted of the creation of a fifth storage location called the 'hole', into

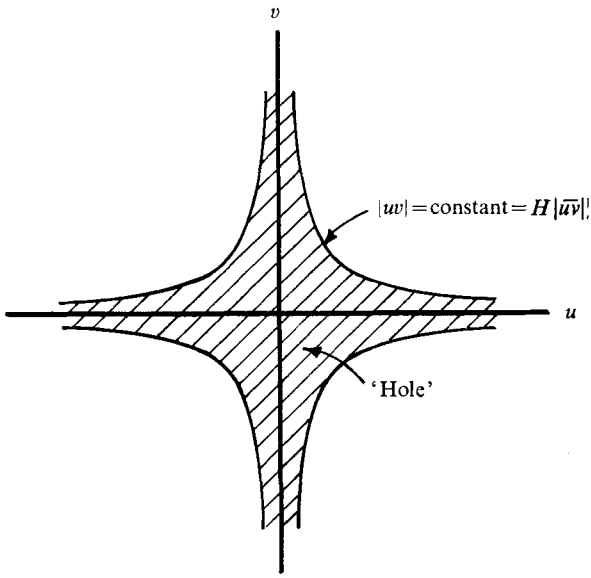

FIGURE 15. Sketch of 'hole' region in uv plane.

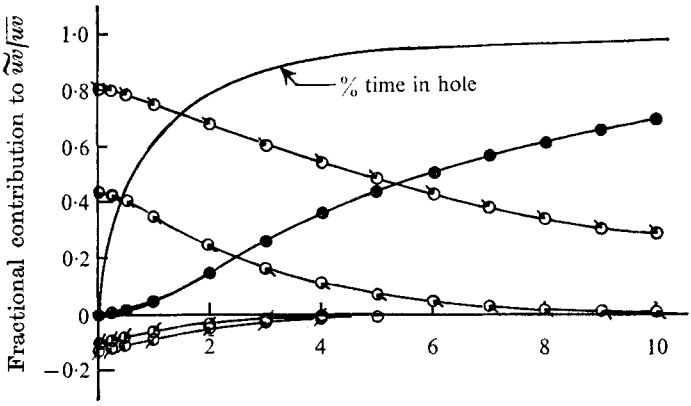

FIGURE 16. Contributions to Reynolds stress from truncated quadrants of u, v plane and percentage time spent in 'hole' as a function of 'hole' size. uv measured at $y^+ = 30$ in low-speed boundary layer; $U_\infty = 19{\cdot}7$ ft/s. Open circles indicate $|uv| >$ hole size: ♂, $u > 0$, $v > 0$; ♁, $u < 0$, $v > 0$; ♀, $u < 0$, $v < 0$; ♀, $u > 0$, $v < 0$. ●, 'hole', $|uv| <$ hole size.

which a digitized value of uv was thrown if for that sample $|uv| < H|\overline{uv}|$. The correlation contributions that remain in the u, v plane are contributions which occur in each quadrant outside a central region bounded by four hyperbolae $|uv| < H|\overline{uv}|$, see figure 15.

Figure 16 shows a plot of the results of the measurements of contributions to $\overline{uv}$ with the hyperbolic central region omitted for various values of the size of the 'hole'. From figure 16, it is clear that the contributions to $\overline{uv}$ from the second quadrant are larger than from any of the others. Furthermore, above the value $|uv| = 5|\overline{uv}|$ essentially all the remaining contributions to $\overline{uv}$ come from the

second quadrant. Also shown on figure 16 is a curve representing the percentage of time that the signal uv remains in the hyperbolic 'hole' $|uv| < H|\overline{uv}|$. Clearly, for a large fraction of the time $|uv|$ is very small relative to shorter intervals of intense activity. Roughly speaking, the intermittency factor for uv (at $y^+ = 30{\cdot}5$) is 0·55 since 55 % of the time the signal uv is in the 'hole', yet the contribution to $\overline{uv}$ that is made by the signal uv while in the 'hole' is small: $(\widetilde{uv}/\overline{uv})_{\text{hole}} = 0{\cdot}01$. The size of the 'hole' for this estimate is $|uv| < 0{\cdot}5\ \overline{uv}$, see figure 16.

4. Summary and discussion of the results of the measurements

In this section the results of the measurements will be discussed and a model for the flow structure of the bursting event that was first presented by Willmarth & Tu (1967) will be discussed in the light of the present measurements. The primary results of the measurements is the demonstration that when u_w becomes sufficiently negative, with negative slope, a burst occurs which makes large contributions to Reynolds stress and production of turbulent energy. The sampled Reynolds stress contributions $\widetilde{uv}$ like those of figure 6 for $u_w < 0$ and negative slope are convected downstream with the local mean speed as our numerous measurements reveal (these measurements are not yet in final form and are not included in this paper). The region occupied by the burst event is long and narrow and appears to grow as it is convected downstream. Furthermore, when $u_w < 0$ with negative slope, sampled measurements of the streamwise component of vorticity were made. These measurements showed that an antisymmetric pattern (in the transverse direction) of streamwise vorticity was present when $u_w < 0$. This is strong evidence that appreciable vorticity is present during the bursting event. The sign of the vorticity is such that an upwelling $v > 0$ of fluid would be expected when $u_w < 0$ with negative slope, and the measurements of $\widetilde{uv}$ reveal that intense bursts 'squirt' low-speed fluid from the region near the wall upward into the higher speed outer flow.

Our earlier measurements (Willmarth & Wooldridge 1963) of the correlation of the pressure field at the wall with velocity components near the wall led us (Willmarth & Tu 1967) to propose that a swept-back pattern of streamwise vorticity in the shape of a hairpin with legs pointing upstream could be responsible for the wall pressure disturbances. We now propose that the same model for the flow structure near the wall is also responsible for the intense bursting events that have been studied by Kim *et al.* (1968), Corino & Brodkey (1969) and here with sampled measurements of $\widetilde{uv}$. Another reason for proposing the model of the hairpin-shaped vorticity is that this configuration of vorticity appears to be the only way an intermittent, very intense, small-scale ejection of fluid could occur. We recall that the onset of the ejection is very abrupt and believe that it must be the result of vortex stretching on (at first) a very small scale in the wall region. Furthermore, it does not seem likely that anything other than an intense local convected pattern of vorticity could be responsible for the highly intermittent signal uv, see figure 13.

Numerous interesting questions remain to be investigated. For example, the question of the nature of the flow disturbance that initiates the bursting event

is still in doubt. Also, the nature of the chaotic interaction observed after the ejection process has become well developed is not understood. Unfortunately, we do not have space here to survey a number of computational results from simplified models of possible flow structures near the wall. We also would like to suggest that the localized flow structure during the bursting event is similar to the organized flow structure that occurs during the creation of a turbulent spot in the transition from laminar to turbulent flow. The initial instability mechanism and the scale of the process that leads to a concentrated localized flow structure during transition may not be the same as it is in the fully developed turbulent boundary layer. However, we propose that the basic flow structure and vorticity pattern that is developed at later stages and the results (creation of Reynolds stress and turbulence) are similar when intermittent and intense contributions to $\overline{uv}$ occur near the wall in the fully developed turbulent boundary layer.

We gratefully acknowledge the financial support of the Fluid Dynamics Branch of the Office of Naval Research. This paper was presented at the NATO–AGARD Fluid Dynamic Panel Specialists Meeting on Turbulent Shear Flows 13–15 September, 1971, in London.

REFERENCES

BLACKWELDER, R. F. & KAPLAN, R. E. 1971 Intermittent structures in turbulent boundary layers. *NATO–AGARD Fluid Dynamics Panel Specialists Meeting on Turbulent Shear Flow*, vol. 3, p. 1.

CLAUSER, F. H. 1956 *Advanced Applied Mechanics*, vol. 4, p. 1. Academic.

COANTIC, M. 1965 *Comptes Rendus*, **260**, 2981.

COLES, D. E. 1954 *Z. angew. Math. Mech.* **5**, 181.

CORINO, E. R. & BRODKEY, R. S. 1969 *J. Fluid Mech.* **37**, 1.

GRASS, A. J. 1971 Structural features of turbulent flow over smooth and rough boundaries. *J. Fluid Mech.* **50**, 233.

KIM, H. T., KLINE, S. J. & REYNOLDS, W. C. 1968 *Thermosciences Division, Dept. Mech. Eng. Stanford University, Rep.* MD-20. (see also 1971 *J. Fluid Mech.* **50**, 133.)

KLINE, S. J., REYNOLDS, W. C., SCHRAUB, F. A. & RUNSTADLER, P. W. 1967 *J. Fluid Mech.* **30**, 741.

KOVASZNAY, L. S. G. 1954 *High Speed Aerodynamics and Jet Propulsion*, vol. IX, article F-2, p. 227. Princeton University Press.

KOVASZNAY, L. S. G., KIBENS, V. & BLACKWELDER, R. F. 1970 *J. Fluid Mech.* **41**, 283.

KOVASZNAY, L. S. G., MILLER, L. T. & VASUDEVA, B. G. 1963 A simple hot-wire anemometer. *Project SQUID Tech. Rep.* JHU-22-P.

LAUFER, J. 1954 *N.A.C.A. Tech. Rep.* no. 1174.

LUMLEY, J. 1970 *Stochastic Tools in Turbulence*, p. 4. Academic.

WALLACE, J. M., ECKELMANN, H. & BRODKEY, R. S. 1972 The wall region in turbulent shear flow. *J. Fluid Mech.* **54**, 39.

WILLMARTH, W. W. & TU, B. J. 1967 *Phys. Fluids*, **9** (suppl.), 134. (See also 1966 *University of Michigan Tech. Rep.* ORA 02920-3-T.)

WILLMARTH, W. W. & WOOLDRIDGE, C. E. 1962 *J. Fluid Mech.* **14**, 187.

WILLMARTH, W. W. & WOOLDRIDGE, C. E. 1963 *AGARD–NATO Rep.* no. 456.